# Modeling and Simulation of a Modified Solar Air Heater Destined to Drying the Gelidium Sesquipedale

Abderrahim El-abidi*,**‡, Said Yadir*,**, Fatima Chanaa**, Mohammadi Benhmida**, Houssam Amiry**, Hamza Bousseta*, Hassan Ezzaki**

*Laboratory of Materials, Processes, Environment, and Quality, the National School of Applied Sciences, Cadi Ayyad University Route Sidi Bouzid, BP 63, 46000, Safi, Morocco

**Laboratory of Electronics, Instrumentation and Energetic, Faculty of Sciences, Chouaïb Doukkali University, B.P 20, El Jadida, Morocco

(a.elabidi@uca.ma, yadir1976@yahoo.fr, fatimachanaa2020@gmail.com, benhmida@gmail.com, houssam.amiry@gmail.com, ezzaki.hassan@gmail.com, hamza.bousseta@gmail.com)

‡Abderrahim El-abidi; Route Sidi Bouzid, BP 63, 46000, Safi, Morocco
Tel: +212 664088042, Fax: +212 24 66 80 12, a.elabidi@uca.ma

*Received: 05.08.2018 Accepted:01.10.2018*

**Abstract-**The open-air solar drying is a traditional method used for drying Gelidium sesquipedale in Morocco, an important commercial maritime specie of red algae existing in abundant quantities in the large Moroccan coast between Safi and EL jadida. However, this method is not professional and is time-consuming. Here, we present a modified design of a solar air heater destined to use as a component in an indirect solar dryer of Gelidium sesquipedale. We report the results of simulation of the thermal behavior of a modified simple back-pass solar collector in order to predict parameters influencing its thermal performances, such as the number and the diameter of perforations in the configuration, the airflow rate, the solar irradiance. To achieve this, a 3D simulation with finite element model (FEM) is built using the meteorological data collected at the chosen location during the regular harvesting period (July, August and September). The results show that the optimal simulated configuration of a flat plate solar collector is of seven symmetrical perforations of 30 mm diameter, and mass airflow rate around 60kg/h. The best conditions for drying algae are achieved using a solar collector facing south and inclined by 20° to the horizontal. The air outlet temperature will be in the range of 35 to 44°C that is relevant for low temperature drying of seven hours a day, safeguarding the quality of the red algae destined for processing.

**Keywords:** red algae, gelidium sesquipedale, numerical simulation, solar collector, solar dryer.

## 1. Introduction

The gelidium sesquipedale is a very important species of red algae and is the basic material of red algae. It is a basic material of the Agar-Agar, a commercial product with gelling powe [1] and having a therapeutic use [2]. The harvesters of this maritime plant located on Morocco's Atlantic coast, between EL Jadida and Safi dry it by direct exposure to sunlight. This traditional and economical drying method permits the conservation and the reduction of the volume and weight of products and therefore diminish storage and transportation costs. Nevertheless, the parameters influencing drying such as solar irradiance, drying airflow rate, ambient temperature, wind velocity, relative air humidity, etc. remain out of control, resulting in a larger drying period, and therefore, an undesirable drying rate. Furthermore, this method can result in quality degradation [3]. Recently several published studies have focused on the drying of plants and foods and maritime species using solar dryers. These studies include drying thymus [4], cocoa beans [5], peeled and unpeeled cherry tomatoes [6], dates [7], Mushrooms [8], bitter gourd [9], pistachio [10], Ghost Chilli Pepper [11],

cashew[12], chilli[13], green chilies , potato chips[14] , marine microalgae[15], Gelidium sesquipedale [16] , etc.

The indirect solar dryer, consists of two main components: a solar air heater collector (SAHC) and a drying chamber. The air is heated using the solar collector before circulating in the drying chamber. The performance of the collector is considerably sensitive to the changes in its design parameters. Therefore, the optimization of the geometrical and physical configuration of a SAHC allows to maximizing the use of sun's thermal energy and obtaining the highest drying rate [17]. Over the past two decades, a number of published articles have been devoted to improving solar air heating collectors by studying and analyzing different collector designs. Leon et al [18] developed unglazed transpired collectors (UTC) also known as perforated collectors. They present the details of a mathematical model for it using heat transfer expressions for the collector components, and empirical relations for estimating the various heat transfer coefficients. Results indicate that the promising thermal performance of (UTC) is relevant for drying of food products and offer itself as an attractive alternate to glazed solar collectors. However, this type of collectors is more used in ventilation applications than in drying ones. Many numerical studies have been done in order to enhance the performance of different types of collectors[19]-[20]. Recently, Orbegoso et al [5] developed a computational fluid dynamics (CFD) based model in order to numerically characterize the thermal performance of (SAHC) submitted under controllable operating conditions. The (CFD) model was employed for three types of SAHC in order to identify the geometric and physical parameters that affect the collectors' thermal performance. The study showed that the three-step (SAHC) having two glasses demonstrated the best thermal performance than that observed in the case of the three-step (SAHC) having three glasses and in the simple – pass one-step (SAHC) of Singh et al. However, this type of collector with two or three step will have the disadvantage of increasing the pressure losses. Ait Mohammed et al[16] studied the kinetic of solar drying of Gelidium sesquipedale. They determined the suitable model for describing the drying curves. The solar dryer used in their work includes than a conventional single cover solar air heater, an auxiliary heating system integrated in the drying chamber. For this reason, they tried drying at higher temperatures (50 and 60°C) and very large volume airflow rates up to 0.0833 $m^3/s$, equivalent to mass airflow rate of 360 *kg/h*. Although the performance of this hybrid equipment is very important for drying, the use of electrical energy in the auxiliary heating system could be considered a disadvantage.

Thus, the objective of this study was to improve a back-pass solar air heater in order to permit a 100% solar drying of plants and agro-food. The thermal behavior of several configurations under forced convection are numerically characterized in order to determine their thermal performance under several controlled operating conditions. The heat transfers by convection and radiation are modeled, and the behavior of the solar collector is simulated to account for its performance for drying Gelidium Sesquipedale in El jadida, by considering the weather conditions during the harvesting period (July, August and September), determined by the Moroccan Ministry of Agriculture and Maritime Fisheries.

## 2. Materiel and Methods

### *2.1 Prototype description*

The air heater collector considered is a simple back-pass; the absorber plate is placed behind an ordinary glass cover with a layer of static air separating it from the cover. The air to be heated flows between the down surface of the absorber and the upper surface of the insulation. For having a good airflow distribution, two perforated barriers are added. The materials considered manufacturing our prototype are ordinary, cheap, and locally available. The synoptic diagram of the collector is shown in Fig. 1. It consists of:

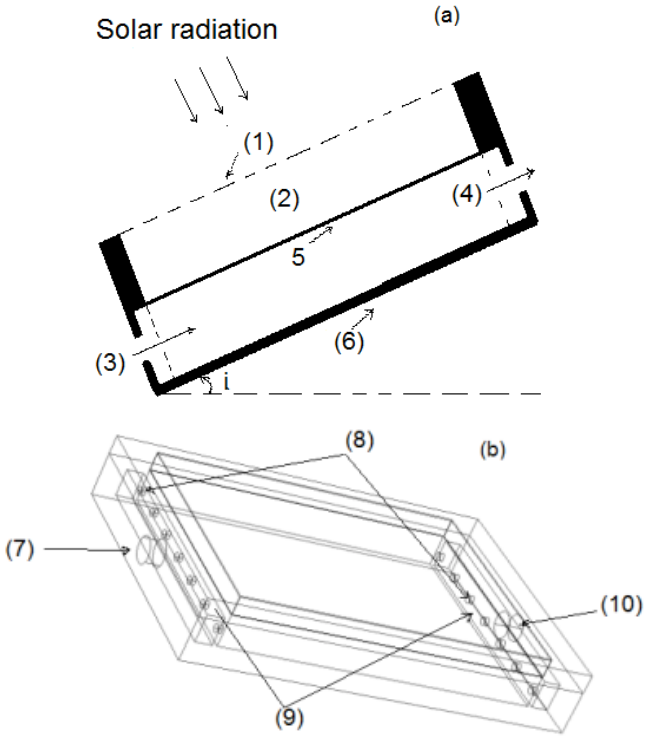


**Fig. 1.** Representations of a solar collector configuration. Longitudinal section (a): glass (1), static air (2), air inlet (3), air outlet (4), absorber(5), thermal insulator(6). 3D view (b): inlet of air (7), internal perforations (8), perforated barriers (9), outlet of air (10).

- A box made of solid wood, of dimensions $(1.440\times1.013\times0.231)m^3$, with openings on the lateral sides of the inlet and the outlet airs.
- An ordinary *4mm* lass that covers the case and ensures the greenhouse effect.

**Table 1.** Parameters assumed in predictions concerning El jadida

| | July | August | September |
|---|---|---|---|
| Wind velocity (m/s) | 4.7 | 4.4 | 4.1 |
| Average monthly ambient temperature (°C) | 23.5 | 23.6 | 22.4 |
| Average monthly atmospheric pressure (kPa) | 100.1 | 100.1 | 100.2 |
| Average monthly relative humidity (%) | 61.8% | 63.3% | 65.9% |

- An absorbent zinc plate whose surface exposed to radiation painted in matte black. The area of the plate is of $(1.170 \times 0.900) m^2$ and the thickness is about $0.8mm$.

- A thermal insulator (expanded polystyrene) at the bottom and on the side of the case, with thickness, respectively, of 43 and 56.5 mm.

- Between the plate and the insulation, the air is distributed using two perforated wooden barriers. Each containing a number $N$ of equidistant perforations, having the same diameter, and distributed symmetrically with respect to the center of the barrier. We choose an odd number $N$ equal to 3, 5, 7, 9, and 11 in order to have the central perforations aligned with the inlet and outlet perforations.

- A fan blowing air inside the collector.

- Two cylindrical pipes of 95 mm diameter are placed at the entrance and at the exit.

The collector is in a fixed position, facing south and inclined by 20° to the horizontal, estimated by iterative numerical calculation on the inclination angle between 0° and 90° and also iteration on the day number $j$ in the year between (152 for July 1st) and (273 for September 30th), for the three months of the harvesting period. The optimal angle 20° is the average of the inclination angles giving the maximum global irradiance at 12H AST (Apparent Solar Time) on the days concerned.

### *2.2 Solar irradiance and meteorological conditions*

In our calculations, we predict solar irradiance Using Meteorological Data[21]. We consider that the ambient temperature, atmospheric pressure, wind velocity and relative humidity are equal to the monthly average values of the three considered months (Table.1.) measured over 22 years between 1983 and 2005 in the area of El Jadida [22].

The existing databases offer only the measured values or the interpolated values of the hourly horizontal global solar irradiance, so we were obliged to estimate them for an inclined plane of an angle of 20°, for clear sky days, according to a semi-empirical model. in our calculations the degradation of solar radiation due to humidity or dust will be taken into account[23]. The direct normal irradiance $I_n$ on a receiving plane normal to this radiation is given by Eq.(1) [24]:

$$I_n = E_{sol} \times \exp(-E_R \times m_a \times T_L) \quad (1)$$

Where $E_{sol}$ the solar constant, is[20]:

$$E_{sol} = 1367 \times \left[1 + 0.0334 \times \cos\left(\frac{360(j - 2.7206}{365.25}\right)\right] \quad (2)$$

The Rayleigh optical thickness $E_R$, can be written from Kasten 's equation, as follows [24]:

$$E_R = 1/\left(0.9 \times m_a + 9.4\right) \quad (3)$$

Where the relative optical air mass $m_a$, is calculated for an altitude of z above sea level [25] as the equation:

$$m_a = \frac{\exp(-0.00011847 \times z)}{\sin(h) + 0.15 \times (3.885 + h)^{(-1.253)}} \quad (4)$$

$h$ is the solar altitude in ($DegC$); and $(z = 10m)$ for EL Jadida .The turbidity factor $T_L$ of Link, is expressed as follows [26]:

$$T_L = 2.4 + 14.6 \times \beta + 0.4 \times (1 + 2\beta) \times \ln(P_v) \quad (5)$$

Where $\beta$ stands for the atmospheric turbidity coefficient of Angstrom [27]. For an urban environment like El jadida $\beta$ is considered equal to 0.1.

$P_v$ is the partial vapor pressure of water in (mbar). The diffuse solar irradiance $I_{dif}$ and $I_r$ reflected from the ground on a receiving plane of inclination are calculated using the following equations [27]:

$$I_{dif} = 125 \times (\sin \mathrm{h})^{0.4} \times (1 + \cos i)/2 \quad (6)$$

$$I_r = 211.86 \times (\sin \mathrm{h})^{1.22} \times (1 - \cos i)/2 \quad (7)$$

The global solar irradiance on an inclined surface with an angle is defined by the following equation [27]:

$$I_G = I_n \times C_I + I_{dif} + I_r \quad (8)$$

and the inclination coefficient is[27],[28]:

$$C_I = \cos\delta \times \cos\omega \times \cos(L_a - i) + \sin\delta \times \sin(L_a - i) \quad (9)$$

Where $L_a$ stands for the site latitude $h$ is the solar altitude; $\omega$ is the hour angle; $\delta$ is the declination; and $i$ is the inclination angle of collector. The global solar irradiance received by the collector was culcuated using all the equations mentioned above, for different hours (AST) of the half day for the three months. The results are shown in Fig. 2(a), Fig. 2(b), and Fig. 2(c).

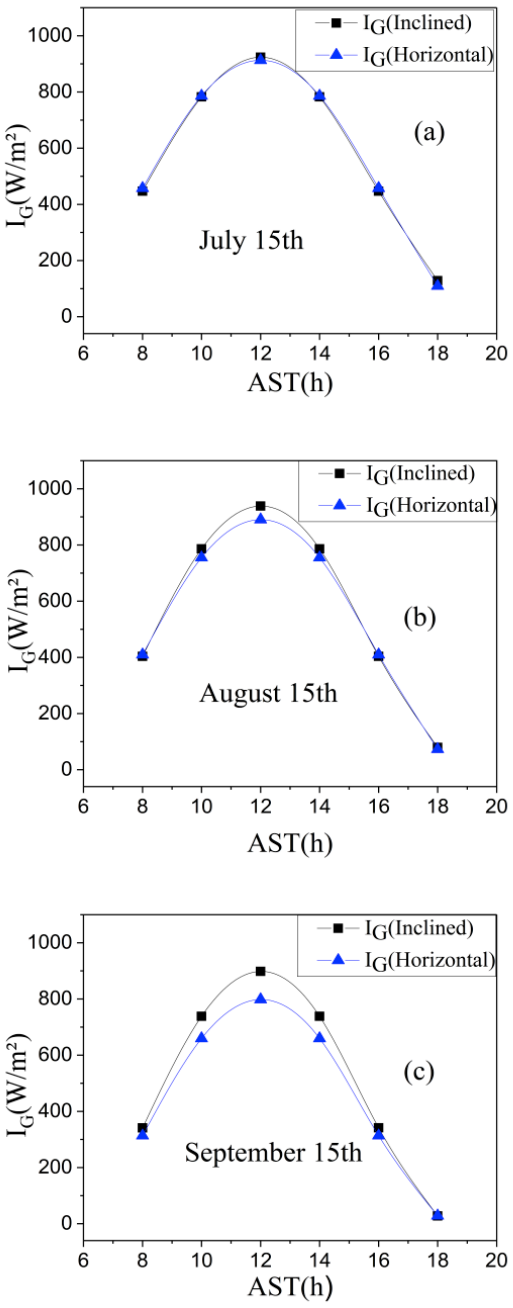


**Fig. 2.** Global solar irradiance received by the glass of the horizontal and inclined collector (20°) versus the apparent solar time hours (AST) rate in different months (a) July 15; (b) August 15; and (c) September 15.

### *2.3 Modeling based on energy balance*

The theoretical calculations are based on the energy balance of the collector are detailed by K. S. Ong [29] and also experimentally validated by him [30]. The energy balance equations of the various collector components per unit area of the collector are written as follows[29]:

- For cover glass:

$$\beta_V \times I_G + h_{ncv}\,(T_{abs} - T_v) + h'_{abs\text{-}v}(T_{abs} - T_v) = U_t\,(T_v - T_a) \quad (10)$$

- For absorber plate:

$$\tau \times \alpha \times I_G = h_{abs\text{-}f}(T_{abs} - T_f) + h_{ncv}\,(T_{abs} - T_v) + h'_d(T_{abs} - T_d) + h'_{abs\text{-}v}(T_{abs} - T_v) \quad (11)$$

- For the airflow:

$$h_{abs-f}(T_{abs} - T_f) = h_{f-d}(T_f - T_d) + P_u \quad (12)$$

- For bottom plate:

$$h_{f-d}(T_f - T_d) + h'_d(T_{abs} - T_d) = U_b(T_d - T_a) \quad (13)$$

Where, $P_u(W/m^2)$ stands for the useful heat transferred to the air per unit area; $\beta_V$ is the absorptivity coefficient of glass; $T_a(°C)$ is the ambient temperature; $T_{abs}(°C)$ is the absorber temperature; $T_v(°C)$ is the glass temperature; $T_f(°C)$ is the airflow temperature; $T_d(°C)$ is the temperature of the bottom of the collector; $T_e(°C)$ is the inlet air temperature; $h_{abs-f}(W.m^{-2}.°C^{-1})$ is the convective heat transfer coefficient between the absorber and the airflow; $h_{f-d}(W.m^{-2}.°C^{-1})$ is the convective heat transfer coefficient between the airflow and the bottom of the collector; $h_{wind}(W.m^{-2}.°C^{-1})$ is the convective heat transfer coefficient between the glass and the wind; $h'_{abs\text{-}v}(W.m^{-2}.°C^{-1})$ is the radiation heat transfer coefficient between the absorber and the glass. $h'_{v-sky}(W.m^{-2}.°C^{-1})$ is the radiation heat transfer coefficient between the glass and the sky; $h'_d(W.m^{-2}.°C^{-1})$ is the radiation heat transfer coefficients between the bottom of collector and the absorber plate; $U_t(W.m^{-2}.°C^{-1})$ is the top heat loss and $U_b(W.m^{-2}.°C^{-1})$ is the bottom heat loss coefficients.

Assuming that $P_u$ is uniform along the collector. This assumption implies that the air temperature varies linearly along the collector and the amount of useful solar irradiance absorbed by the collector, converted into heat, and received by the circulating air can be written as follows [29]:

$$P_u = \frac{D_m \times c}{L \times l} \times (T_s - T_e) \quad (14)$$

Where, $D_m$ is the mass airflow rate $L$ is the length of the absorber flat zinc plate $l$ is the width of the absorber flat zinc plate and $c$ is the specific heat capacity of air.

The average airflow temperature is approximated by[29]:

$$T_f = (T_s + T_e)/2 \quad (15)$$

From where: $$P_u = \frac{2D_m \times c}{L \times l} \times (T_f - T_e) \quad (16)$$

With: $\Gamma = \frac{2D_m \times c}{L \times l}$ We get: $P_u = \Gamma \times (T_f - T_e)$ (17)

By substituting the Eq.(16) in the Eq.(12) and rearranging, we obtain the following equations:

$$(h_{ncv}+h'_{abs\text{-}v}+U_t)\,T_v-(h_{ncv}+h'_{abs\text{-}v})\,T_{abs}-U_t\times T_a-\beta\times I_G=0 \quad (18)$$

$$-(h_{ncv}+h'_{abs\text{-}v})\,T_v+(h_{ncv}+h_{abs\text{-}f}+h'_d+h'_{abs\text{-}v})T_{abs}-h_{abs\text{-}f}\times T_f-h'_d\times T_d-\tau\times\alpha\times I_G=0 \quad (19)$$

$$h_{abs\text{-}f}\times T_{abs}-(h_{abs\text{-}f}+h_{f\text{-}d}+\Gamma)\,T_f+h_{abs\text{-}d}\times T_d+\Gamma\times T_e=0 \quad (20)$$

$$h'_d\times T_{abs}+h_{f\text{-}d}\times T_f-(h_{f\text{-}d}+h'_d+U_b)\times T_d+U_b\times T_a=0 \quad (21)$$

The convective heat transfer coefficient $h_{wind}$ between the glass and the wind can be determined from the correlation [31]:

$$N_u=0.0723\times \mathrm{Re}^{0.773}\times \mathrm{Pr}^{1/3} \quad (22)$$

Where, $N_u$ is the Nusselt number, $\mathrm{Re}$ is the Reynolds Number, and $\mathrm{Pr}$ is the Prandtl number. Moreover:

$$h_{wind}=N_u\times k/L \quad (23)$$

The sky temperature $T_{sky}$ is given by [29]:

$$T_{sky}=0.0552\times(Ta)^{1.5} \quad (24)$$

The Eq. (25), Eq. (26) and Eq.( 27) give the radiation heat transfer coefficients as follows:

$$h'_{v-sky}=\sigma\times\varepsilon_v(T_v{}^2+T_{sky}^2)(T_v{}^2-T_{sky}^2)/(T_v-T_a) \quad (25)$$

$$h'_{abs-v}=\frac{\sigma}{\frac{1}{\varepsilon_{abs-u}}+\frac{1}{\varepsilon_v}-1}(T_{abs}^2+T_v{}^2)(T_{abs}+T_v) \quad (26)$$

$$h'_d=\frac{\sigma}{\frac{1}{\varepsilon_{abs-d}}+\frac{1}{\varepsilon_d}-1}(T_{abs}^2+T_d{}^2)(T_{abs}+T_d) \quad (27)$$

The Eq. (28) and Eq. (29) give the top heat loss coefficient and the bottom heat loss coefficient, respectively:

$$U_t=h_{wind}+h'_{v-sky} \quad (28)$$

$$U_b=1/\left[1/\left(e_{pol}/k_{poly}\right)+\left(1/h_{wind}\right)\right] \quad (29)$$

Where, $e_{pol}(m)$ is the insulation thickness (polystyrene) and $k_{poly}(W/m.K)$ is the thermal conductivity of polystyrene.

Forced convection coefficient between two parallel plates in case of turbulent airflow given by Sider and Tate as [18]:

$$Nu=0.027\times \mathrm{Re}^{0.8}\times \mathrm{Pr}^{0.3}\times\left(\mu/\mu_w\right)^{0.14} \quad (30)$$

Where, $\mu_w\left(Pa.s\right)$ is the viscosity of air evaluated at the wall temperature and $\mu\left(Pa.s\right)$ is the dynamic viscosity of air

Sider and Tate, also give the natural convection coefficient $h_{ncv}$ between two parallel plates as follows [18]:

$$h_{ncv}=0.2\times(L/h_1)^{-1/9}\times(Gr\times \mathrm{Pr})^{0.33} \quad (31)$$

Where,

$h_1$ is the separation distance between the glass and the absorber plate and $Gr$ is the Grashof number.

The physical properties of air density, specific heat, dynamic viscosity, and thermal conductivity are given respectively with the following equations [29], where T is expressed in (°C):

$$\rho_{air}(T)=1.1774-0.00359\times(T-27) \quad (32)$$

$$Cp(T)=1.005755.10^3+6.6.10^{-5}(T-27) \quad (33)$$

$$\mu(T)=1.983.10^{-5}+1.84.10^{-8}\times(T-27) \quad (34)$$

$$k(T)=2.624.10^{-2}+7.58.10^{-5}\times(T-27) \quad (35)$$

According to continuity equation in fluid mechanics (conservation of mass) [32], the air velocity $v_i$ exiting the interior perforations was estimated by Eq. (36):

$$S_0\times v_0=\sum_{i=1}^{N}\left(S_i\times v_i\right) \quad (36)$$

$S_0$ and $S_i$ are the area of external inlet perforation and the internal inlet perforation, respectively.

$v_0$ and $v_i$ are initial air velocity and the air velocity after crossing the barrier, respectively.
Since[32],

$$D_m=S_0\times V_0/\rho_{air} \quad (37)$$

Assuming that the air is distributed identically through the $N$ perforations, we get the following equation:

$$v_i=D_m/\left[N\times\rho_{air}\times T_{amb}\times\pi d_i^2\right] \quad (38)$$

The global thermal efficiency $\eta_T$ of the collector is as follows[17]:

$$\eta_T=P_u/I_G \quad (39)$$

Since our solar air heater is assumed as a short collector (1.17m) so as demonstrated by K. S. Ong [29] we do not need to divide it into a finite number of short collectors. Therefore, the wall temperatures are assumed uniform and the air temperatures are assumed to vary linearly along the collector in the direction of airflow. The Eq. (18), Eq. (19), Eq. (20) and Eq. (21) form a system of non-linear equations to four unknowns: $T_v$, $T_{abs}$, $T_f$ and $T_d$. The resolution method of this system is different from the one used by K.S.Ong. We used the optimization toolbox in MATLAB software allowing us to calculate accurately the values of $T_{sc}$.the optimization algorithm is the trust-region-dogleg algorithm, the Maximum number of iterations allowed is equal to 400, and all termination tolerances are equal to the default value of $10^{-6}$.

### *2.4 Three dimensional FEM model*

To simulate the behavior of the system, a 3D simulation with finite element model (FEM) is built. We took into consideration the simultaneous thermal interaction of the seven union domains (static air, airflow, down insulator, lateral insulator, absorber plat, and glass). The behavior of the collector has been studied under stationary operating conditions. The equation governing heat transfer is given by [33]:

$$\rho \times Cp \times u \nabla T = \nabla.(k \nabla T) + Q \quad (40)$$

Where, $T(K)$ is the Absolut temperature of the solid or fluid material; $\rho(kg/m^3)$; is the density of the material the solid or fluid $C_p(J.kg^{-1}.°C^{-1})$ is the specific heat capacity at constant pressure of the solid or fluid material; $u(m/s)$ is the Eulerian velocity of a fluid particle $Q(J)$ is the Heat Sources.

The equations governing the airflow for a Newtonian low compressible fluid, in turbulent airflow, are defined In the RANS (Reynolds Averaged Navier-Stokes-) approach[32], by the following equations[33]:

$$\rho_{air} \times (u.\nabla)u = -\nabla p + \nabla.[(\mu + \mu_T)((\nabla u + (\nabla u)^T) - \frac{2}{3}(\nabla.u)I)] + \rho_{air} \times g \quad (41)$$

$$\rho_{air} \times (\nabla u) = 0 \quad (42)$$

Where, $p(Pa)$ is the Thermodynamic pressure of air; $I$ is the Tensor unit; $g(m/s^2)$ is the Gravity; $k(W/m.k)$ is the coefficient of thermal conduction; $\rho(kg/m^3)$ is the density of the material; $\rho_{air}(kg/m^3)$; is the density of air $\mu(Pa.s)$ is the dynamic viscosity of air and $\mu_T(Pa.s)$ is the turbulence viscosity of air.

The radiation heat exchange between a surface and its environment is given by the following equation:

$$q = \varepsilon_s \times \sigma \times (T_a^4 - T_s^4) \quad (43)$$

With $\varepsilon_s$ and $\sigma$ are the surface emissivity and Stefan-Boltzmann constant, respectively

The radiation heat exchange between two parallel surfaces 1 and 2 is given by [33]:

$$q = \frac{\sigma}{(1/\varepsilon_1) + (1/\varepsilon_2) - 1} \times (T_1^4 - T_2^4) \quad (44)$$

The emissivity $\varepsilon_i$ of the materials used[34], are given in Table 2.

**Table 2.** Emissivity in infrared thermography of some Materials considered in predictions.

| Material | Ordinary glass (4mm) | Plate of natural Zinc | Oil paint matt | Expanded polystyrene |
|---|---|---|---|---|
| Emissivity $\varepsilon_i$ | 0.92 | 0.18 | 0.95 | 0 |

The flow chart in Fig. 3 shows the steps involved in the simulation study. The partial differential equations shown earlier in this section must be discretized into a set of algebraic equations, which may be solved based on the finite element method (FEM). The simulations of the seven geometrical domains are discretized into tetrahedral elements. Since the most important energy exchanges take place at the absorber level, we have increased the fineness of our mesh size of absorber boundaries by choosing a mesh triangular type extremely fine. The number of elements is 273942 domain elements, 52641 boundary elements, and 3646 edge elements. Such number of mesh elements permits to have more precision on results (Fig. 4) although it requires a much longer computation time. The relative tolerance was fixed at $10^{-3}$.

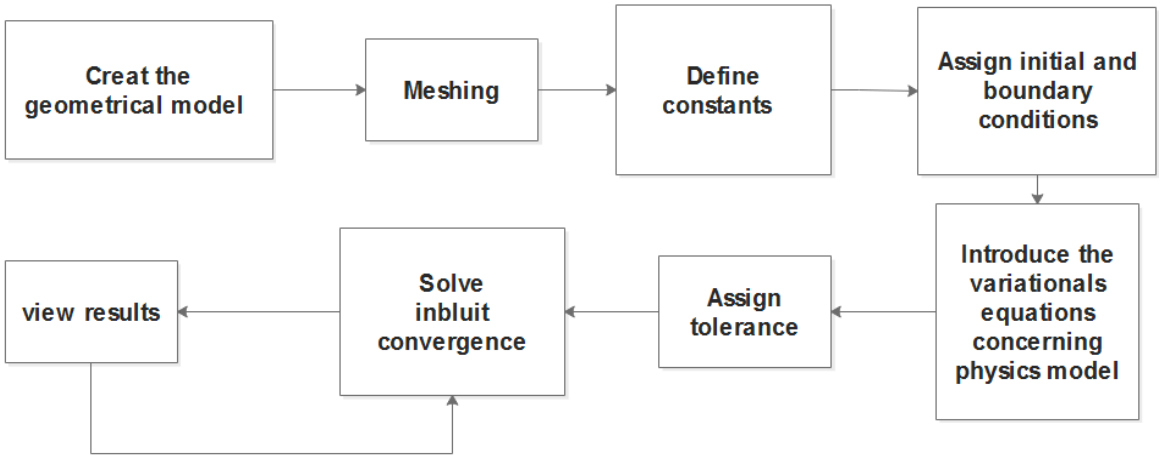


**Fig. 3.** Flow chart for the simulation study

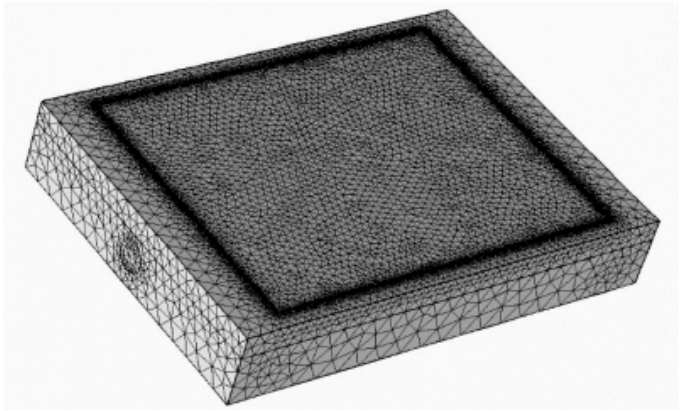

**Fig. 4.** The mesh type

## 3. Results and Analysis

### *3.1 Validation of the numerical simulation model*

Figures 5 (a), 5 (b), and 5(c) represent the variation of the outlet simulated $T_s$ using the FEM model and the outlet calculated temperature $T_{sc}$ using the energy balance, versus the mass airflow rate for the prototype with seven perforations, a diameter of 30mm, and under the same conditions. Its show that the two results are in good agreement and the discrepancies in all cases are less than $1°C$. This result permits to valid the three-dimensional FEM simulation model and then to use it to simulate several further configurations by changing the number or the diameters of perforations in order to identify which one demonstrated the best thermal performance.

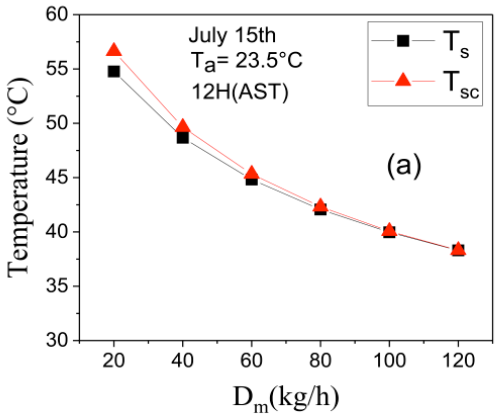


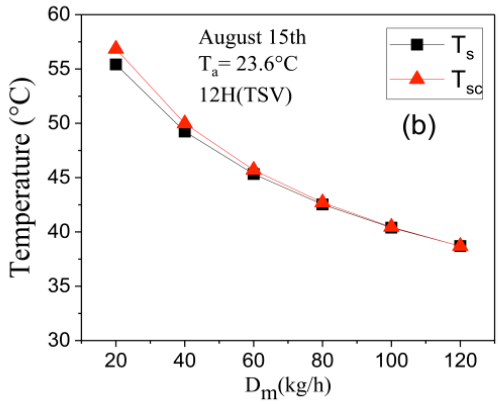


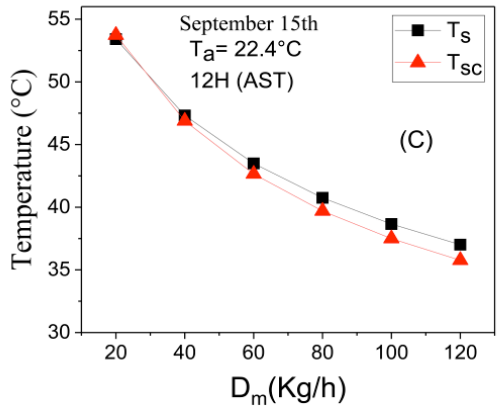


**Fig. 5.** Outlet air temperatures $T_s$ and $T_{sc}$ versus mass airflow rate in different months (a) July 15; (b) August 15; and (c) September 15.

### *3.2 Optimization of the performance of the prototype of collector*

For a constant airflow rate, the global thermal efficiency of a solar collector is a linear function of the air temperature rise between its outlet and inlet $\Delta T = T_s - T_e$. Therefore, we considered comparing the thermal performance of different solar collector configurations under the same operating

condtions: $I_G = 800W/m^2, T_e = T_a = 25°C, v_{wind} = 5.6m/s$ and $D_m = 60kg/h$ by comparing their $\Delta T$. Since the glazing is the same for all configurations, a comparison is carried out without glazing to reduce simulation computing time and make a finer mesh for more accurate results.

The effect of the perforation diameter was studied by considering three different diameters (30, 35, 40 mm). The calculations of pressure losses (Fig.6) show that these only depend on the collector configuration and decrease when the number of perforations increases. Pressure losses vary moderately for perforations between *N=7* and *N=11*.

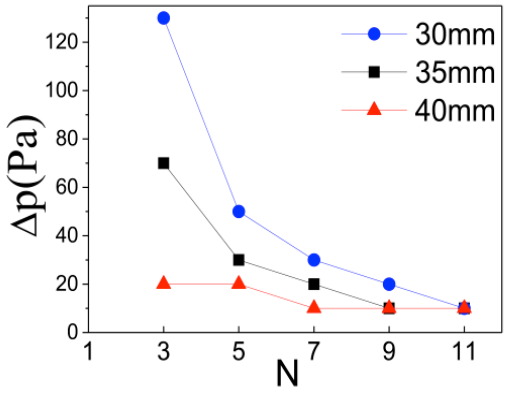


**Fig. 6.** Pressure losses in the collector versus number and diameters of perforations

As illustrated in the Fig.7, the results show that the thermal performance of the collector increases as the diameter of perforation decreases. It is clear that a prototype solar collector with seven perforations with diameters equal to 30mm is more interesting as a prototype solar collector with a single pass under absorber. A diameter of less than 30mm seems undesirable since the pressure drop becomes very high as illustrated in Fig. 6. The calculated air temperature rise of the collector without perforated barrier is of $\Delta T = 5°C$ which is twice as small as $\Delta T$ in the optimal configuration. This confirms the improvement of the simple Back-pass collector by adding the two perforated barriers to the design.

Physically, we can explain the shape of the curve in Fig.7 by comparing the effect of air distribution and the effect of turbulence produced by $N$ perforations. While $N$ is less than seven, the air flow distribution improves progressively with the increase of their number, so improves the heat transfer by convection with the absorber. At the same time, decreases the velocity $v_i$ of the air outlet from the perforations and consequently, will decrease the turbulence, which will result in the decrease of this transfer. In fact, the shape of the curve could be explained for $N$ less than seven by the predominance of the effect of air distribution on the turbulence effect, which is decreasing. From $N = 7$ to N=11, the effect of reduced turbulence predominates, especially as the improvement in air distribution becomes less and less important.

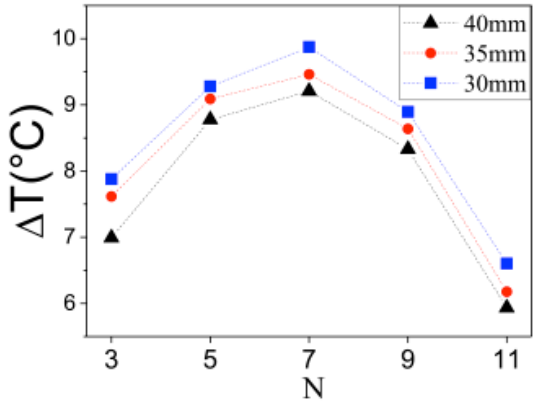


**Fig. 7.** Air temperature rise versus the number of perforations N for different perforation diameters

The decrease of the diameter of the perforations $d_i$ will increase the velocity of the airflow and consequently, will increase the turbulence, from where the improvement of the heat transfer between the air and the absorber.

All these results are in agreement with the results obtained from the variation of pressure losses $\Delta p$ in the solar collector versus *N,* where Δp decreases gradually from *3* to *7* and remains almost constant from *N=7*. The decrease in diameter $d_i$ reduces pressure losses and improves air distribution and turbulence, which means improved the thermal transfer with the absorber plate.

Fig. 8. shows the evolution of $\Delta T$ as a function of the ratio $1/d_i^2$. The statistical determination coefficient $R^2$ is calculated for the two entities. The obtained values are near *1*, that confirm a strong linear correlation between $1/d_i^2$ and $\Delta T$ for a given configuration with *N* perforations (Table 3).

**Table 3.** The Determination coefficient $R^2$ for different configurations of air collectors

| $N$ | 3 | 5 | 7 | 9 | 11 |
|---|---|---|---|---|---|
| $R^2$ | 0.941 | 0.965 | 1.000 | 0.985 | 1.000 |

The simulation, in the stationary state, using the three-dimensional FEM model, allows evaluating the average of outlet air temperature $T_S$, the average absorber temperature $T_{abs}$, the average glass temperature $T_v$ (Fig. 9). It is clear that all these temperatures decrease with increasing airflow rate. This result can be explained by the increasing of the amount of air passing through the collector per unit time.

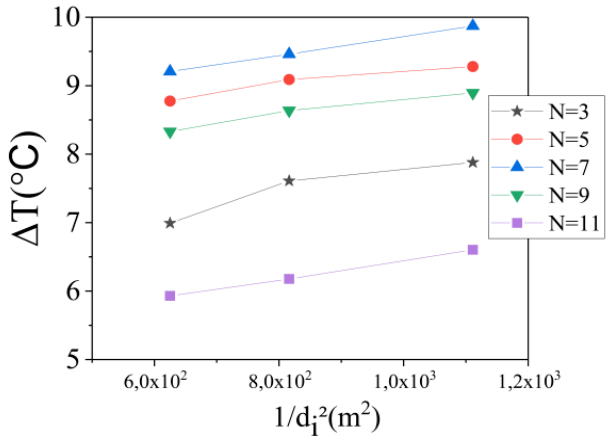


**Fig. 8.** Air temperature rise versus the ratio $1/d_i^2$

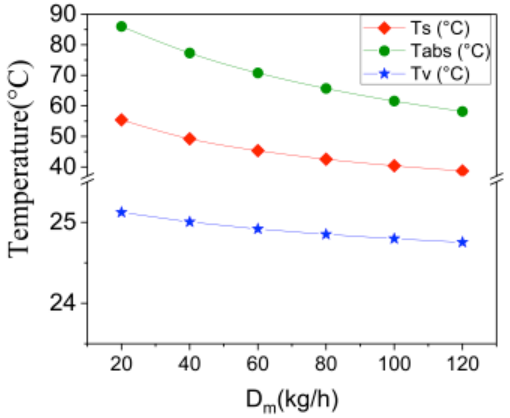


**Fig. 9.** Temperatures of the outlet air, the absorber, and the glass versus the mass airflow rate

The calculation of the global thermal efficiency of the collector (Fig. 10) shows that the thermal efficiency increases with increasing mass airflow. We explain that with the increase of the turbulence effect, that improve the convective exchange between the flowing air and the absorbent plate. The figures 10 shows that the correlation between efficiency and airflow rate is not linear because airflow is implicitly temperature-dependent. Indeed, $\Delta T$ Decreases with the increase of $D_m$. The choice of the solar collector's operating airflow rate will therefore be a compromise between a higher air temperature rise and a higher thermal efficiency.

The solar irradiance in the clear sky hypothesis is symmetrical (Fig. 3(a), Fig.3(b) and Fig 3.(c)) so we decided to do the simulation calculations for half-day only. The simulation results shown in Fig.11(a), Fig.11(b) and Fig.11(c) illustrates the behavior of the solar collector in the stationary case during three trial days of the regular harvesting period of *Gelidium sesquipedale*. Since the air outlet temperature and the global efficiency of the solar collector varies in opposite ways with respect to the mass airflow, a compromise between the two parameters is required. Therefore, we fixed the operating airflow rate in the range $(60 \pm 5) kg/h$ allowing a sufficient global efficiency approximately equal to 50% and a sufficient drying air temperature in all cases between 35°C and 44°C for a duration of approximately seven continuous hours per day from 9h (AST) to 16h (AST).

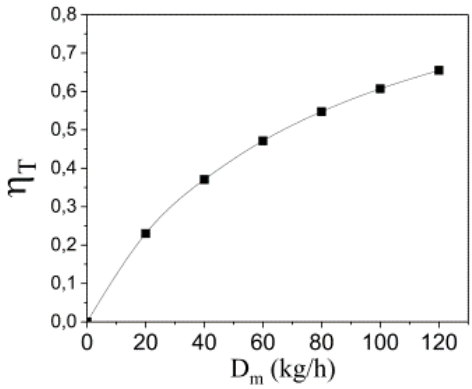


**Fig. 10.** Global collector efficiency versus mass airflow rate

*3.3 Study of an eventual use in drying Gelidium sesquipedale*

## 4. Conclusion

The objective of the work was to propose a modified configuration of a solar air heater and to determine the parameters allowing operation capable of meeting the thermal requirements necessary to reduce the drying time of the *Gelidium sesquipedale* in El Jadida in Morocco. The following conclusion can be drawn as follows:

✓ The FEM model was successfully validated through comparison with the calculations using the energy balance equations. Results obtained by the two approaches are comparable.

✓ A simple back-pass solar collector with seven perforations per barrier with a diameter of 30 mm is interesting and allows relatively a higher thermal performance in comparison with the other modified and the unmodified geometries.

✓ Considering the clear sky assumption, the use of our air heater prototype as a component in a solar dryer of Gelidium sesquipedale, is possible for approximately seven hours of continuous operation per day during the regular harvesting period. The collector must be facing south, inclined by 20° to the horizontal in order to increase the energy absorbed, and consequently improve red algae drying conditions. For a mass airflow rate of about 60kg/h the air outlet temperature will be between 35°C and 44°C relevant for low temperature drying.

✓ The present study will permit the application of this collector to study experimentally the low temperature drying kinetics of *Gelidium sesquipedale* using a purely solar dryer without any electrical energy supply.

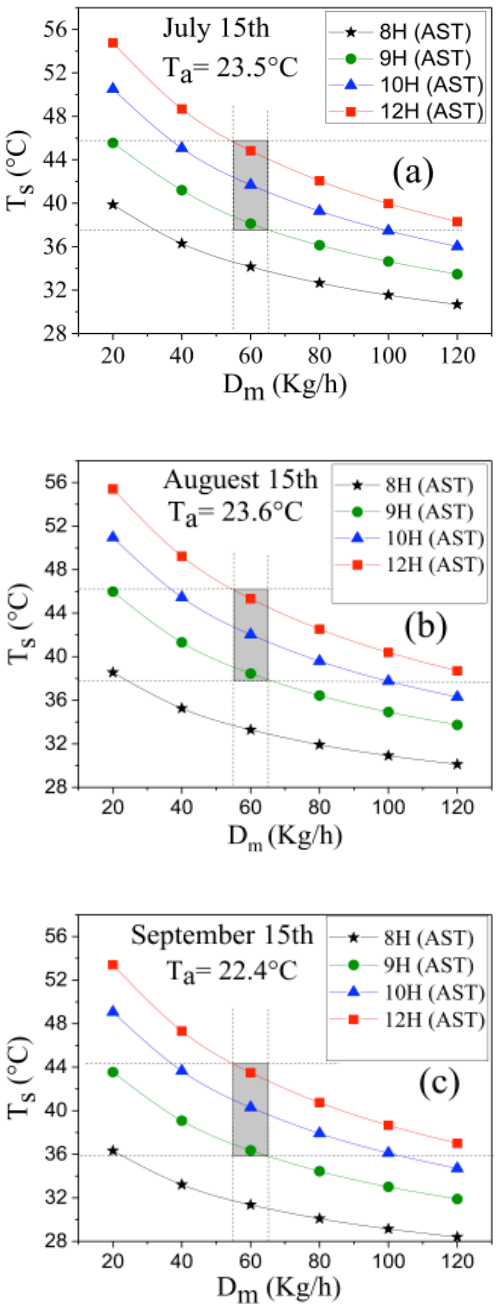


**Fig. 11.** Outlet air temperature versus mass airflow rate at different operating hours in different months (a) July15 (b); August 15; and (c) September 15

## References

[1] M. R. Vignon, C. Rochas, R. Vuong, P. Tekely, and H. Chanzy, "Gelidium sesquipedale (Gelidiales, Rhodophyta) Π. An Ultrastructural and Morphological Study," *Bot. Mar.*, vol. 37, p. 10, 1994.

[2] O. Iglesias and J. L. Bueno, "Water agar-agar equilibrium: determination and correlation of sorption isotherms," *Int. J. Food Sci. Technol.*, p. 8, 1999.

[3] M. Kumar, S. K. Sansaniwal, and P. Khatak, "Progress in solar dryers for drying various commodities," *Renew. Sustain. Energy Rev.*, vol. 55, pp. 346–360, Mar. 2016.

[4] A. A. El-Sebaii and S. M. Shalaby, "Experimental Investigation of Drying Thymus Cut Leaves in Indirect Solar Dryer With Phase Change Material," *J. Sol. Energy Eng.*, vol. 139, no. 6, p. 061011, Sep. 2017.

[5] E. M. Orbegoso, R. Saavedra, D. Marcelo, and R. La Madrid, "Numerical characterisation of one-step and three-step solar air heating collectors used for cocoa bean solar drying," *J. Environ. Manage.*, vol. 203, pp. 1080–1094, Dec. 2017.

[6] L. Bennamoun, R. Khama, and A. Léonard, "Convective drying of a single cherry tomato: Modeling and experimental study," *Food Bioprod. Process.*, vol. 94, pp. 114–123, Apr. 2015.

[7] S. Manaa, M. Younsi, and N. Moummi, "Study of Methods for Drying Dates; Review the Traditional Drying Methods in the Region of Touat Wilaya of Adrar-Algeria," *Energy Procedia*, vol. 36, pp. 521–524, 2013.

[8] A. Reyes, A. Mahn, and F. Vásquez, "Mushrooms dehydration in a hybrid-solar dryer, using a phase change material," *Energy Convers. Manag.*, vol. 83, pp. 241–248, Jul. 2014.

[9] S. Vijayan, T. V. Arjunan, and A. Kumar, "Mathematical modeling and performance analysis of thin layer drying of bitter gourd in sensible storage based indirect solar dryer," *Innov. Food Sci. Emerg. Technol.*, vol. 36, pp. 59–67, Aug. 2016.

[10] A. Midilli, "Determination of pistachio drying behaviour and conditions in a solar drying system," *Int. J. Energy Res.*, vol. 25, no. 8, pp. 715–725, Jun. 2001.

[11] D. K. Rabha, P. Muthukumar, and C. Somayaji, "Experimental investigation of thin layer drying kinetics of ghost chilli pepper (Capsicum Chinense Jacq.) dried in a forced convection solar tunnel dryer," *Renew. Energy*, vol. 105, pp. 583–589, May 2017.

[12] S. Dhanushkodi, V. H. Wilson, and K. Sudhakar, "Mathematical modeling of drying behavior of cashew in a solar biomass hybrid dryer," *Resour.-Effic. Technol.*, vol. 3, no. 4, pp. 359–364, Dec. 2017.

[13] Mahendra S. Seveda, "Design of a Photovoltaic Powered Forced Convection Solar Dryer in NEH Region

of India," *International Journal of Renewable Energy Research*, p. Vol. 3, No. 4, 2013.

[14] D. Parikh and G. D. Agrawal, "Solar Drying In Hot and Dry Climate of Jaipur, India," *International Journal of Renewable Energy Research*, p. Vol. 1, N.4, 224-231, 2011.

[15] M. Aziz, T. Oda, and T. Kashiwagi, "Energy-efficient algae utilization based on enhanced process integration," *2013 International Conference on Renewable Energy Research and Applications (ICRERA)*, Madrid, Spain, pp. 395–400, Oct-2013.

[16] L. Ait Mohamed, C. S. Ethmane Kane, M. Kouhila, A. Jamali, M. Mahrouz, and N. Kechaou, "Thin layer modelling of Gelidium sesquipedale solar drying process," *Energy Convers. Manag.*, vol. 49, no. 5, pp. 940–946, May 2008.

[17] F. Jafarkazemi and E. Ahmadifard, "Energetic and exergetic evaluation of flat plate solar collectors," *Renew. Energy*, vol. 56, pp. 55–63, Aug. 2013.

[18] M. A. Leon and S. Kumar, "Mathematical modeling and thermal performance analysis of unglazed transpired solar collectors," *Sol. Energy*, vol. 81, no. 1, pp. 62–75, Jan. 2007.

[19] Mohamed H. Ahmed, Alberto Giaconia, and Amr M. A. Amin, "Effect of solar collector type on the absorption system performance," *2017 IEEE 6th International Conference on Renewable Energy Research and Applications (ICRERA)*, San Diego, CA, USA, 05-Nov-2017.

[20] O. K. A. Ahmed, "Assessment of the Performance for a New Design of Storage Solar Collector," *International Journal of Renewable Energy Research*, p. Vol.8, No.1, Mar-2018.

[21] M. Demirtas, M. Yesilbudak, S. Sagiroglu, and I. Colak, "Prediction of solar radiation using meteorological data," in *2012 International Conference on Renewable Energy Research and Applications (ICRERA)*, Nagasaki, Japan, 2012, pp. 1–4.

[22] Surface meteorology and Solar Energy, "A renewable energy resource web site (release 6.0)." (https://eosweb.larc.nasa.gov/.

[23] Ahmad M.A.M. Serag Eldin et al, "Effect of dust deposition on performance of thin film photovoltaic Module in Harsh Humid Climate," *2013 Int. Conf. Renew. Energy Res. Appl. ICRERA*, pp. 674–679, Oct. 2013.

[24] M. A. Abdelrahman, S. A. M. Said, and A. N. Shuaib, "Comparison between atmospheric turbidity coefficients of desert and temperate climates," *Sol. Energy*, vol. 40, no. 3, pp. 219–225, 1988.

[25] D. Djafer and A. Irbah, "Estimation of atmospheric turbidity over Ghardaïa city," *Atmospheric Res.*, vol. 128, pp. 76–84, Jul. 2013.

[26] A. Louche, G. Peri, and M. Iqbal, "An analysis of linke turbidity factor," *Sol. Energy*, vol. 37, no. 6, pp. 393–396, 1986.

[27] C. P. De Brichambaut and C. Vauge, *Le gisement solaire : évaluation de la ressource énergétique*, Tec et doc. Paris- France, 1982.

[28] M. Jazayeri, S. Uysal, and K. Jazayeri, "A case study on solar data collection and effects of the sun's position in the sky on solar panel output characteristics in Northern Cyprus," in *2013 International Conference on Renewable Energy Research and Applications (ICRERA)*, Madrid, Spain, 2013, pp. 184–189.

[29] K. S. Ong, "Thermal performance of solar air heaters: mathematical model and solution procedure," p. 17, 1995.

[30] K. S. Ong, "Thermal performance of solar air heaters experimental correlation," *Solar Energy*, pp. 209–220, 1995.

[31] A. V. Rabadiya and R. Kirar, "Comparative Analysis of Wind Loss Coefficient (Wind Heat Transfer Coefficient) For Solar Flat Plate Collector.," vol. 2, no. 9, p. 6, 2012.

[32] J. H. Ferziger and M. Perić, *Computational methods for fluid dynamics*, 3rd, rev. ed ed. Berlin ; New York: Springer, 2002.

[33] R. Bird, W. E. Stewart, and E. N. Lightfoot, *Transport phenomena*, 2nd, Wiley international ed ed. J. Wiley, 2002.

[34] Thermography infrared, "http://www.thethermograpiclibrary.org." 01-Jul-2017.